Published for SISSA by Springer

Received: November 9, 2022
Revised: January 27, 2023
Accepted: February 23, 2023
Published: March 13, 2023

Transverse momentum resummation at N^{3}LL+NNLO for diboson processes

John M. Campbell,[a] **R. Keith Ellis,**[b] **Tobias Neumann**[c] **and Satyajit Seth**[d]

[a] *Fermilab,*
PO Box 500, Batavia IL 60510-5011, U.S.A.
[b] *Institute for Particle Physics Phenomenology, Durham University,*
Durham, DH1 3LE, U.K.
[c] *Department of Physics, Brookhaven National Laboratory,*
Upton, New York 11973, U.S.A.
[d] *Physical Research Laboratory,*
Navrangpura, Ahmedabad — 380009, India
E-mail: johnmc@fnal.gov, keith.ellis@durham.ac.uk, tneumann@bnl.gov, seth@prl.res.in

Abstract: Diboson processes are one of the most accessible and stringent probes of the electroweak gauge structure of the Standard Model at the LHC. They will be probed at the percent level at the high-luminosity LHC, challenging current theory predictions. We present transverse momentum resummed calculations at N^{3}LL+NNLO for the processes ZZ, WZ, WH and ZH, compare our predictions with most recent LHC data and present predictions at 13.6 TeV including theory uncertainty estimates. For W^+W^- production we further present jet-veto resummed results at N^{3}LL$_\mathrm{p}$+NNLO. Our calculations will be made publicly available in the upcoming MCFM release and allow future analyses to take advantage of improved predictions.

Keywords: Higher-Order Perturbative Calculations, Resummation

ArXiv ePrint: 2210.10724

https://doi.org/10.1007/JHEP03(2023)080

JHEP03(2023)080

Contents

1 Introduction

Large experimental efforts at the LHC are dedicated to the analysis of Standard Model (SM) electroweak gauge bosons. The production of γ, W, Z and H are typically considered either alone or in pairs, see table 1 for analyses of diboson processes at 13 TeV. Recent developments include evidence for the triboson processes [1–3]. The standard treatment of all these processes exploits the collinear factorization theorem to combine parton distribution functions (PDFs) and a hard scattering cross-section evaluated at a scale close to Q to derive a prediction. The scale Q is the invariant mass of the produced colorless final state. These collinear factorization predictions are not appropriate at small transverse momentum q_T, where predictions at a fixed order of α_s contain powers of $L = \log(Q^2/q_T^2)$. In addition, for the same reason, collinear factorization predictions are not suitable for cross-sections where jet activity is vetoed. In the region of small transverse momentum the fixed-order predictions need to be enhanced with resummation of these logarithms to all orders in α_s. This necessitates an improved power counting where $\log(Q^2/q_T^2) \sim 1/\alpha_s$ and exploits a factorization theorem at small q_T, valid up to terms suppressed by some power of q_T/Q.

Since the dominant fraction of cross-section resides at low transverse momentum, accurate theoretical control of this region is important. In addition, precise resummed predictions are necessary to validate the transverse-momentum spectra obtained from parton shower event generators operating at a lower logarithmic accuracy. Compared to single boson production, resummation effects for boson pair processes are expected to be even more important at the same value of q_T because the value of Q is much larger.

JHEP03(2023)080

Process	ATLAS	CMS
WZ	[19]	[20–22]
ZZ	[23, 24]	[25]
WW	[26, 27]	[21, 28]
WH/ZH	[29, 30]	[31]

Table 1. Experimental publications for boson pair production at 13 TeV.

Of all massive diboson processes, the production of W^+W^- has received most theoretical and phenomenological attention. This is because of its sizable cross-section and its role as a background to top-quark production and to Higgs-boson production. Transverse momentum resummation in W^+W^- processes has been considered in refs. [4–7]. In particular ref. [7] discusses the resummation of transverse momentum logarithms at N^{2}LL+NNLO. The important topic of the resummation of jet veto logarithms in W^+W^- processes has been considered in refs. [7–10].

As for the other processes, ref. [11] considers the $W^\pm Z$ and ZZ processes (as well as W^+W^-) at N^{2}LL+NLO. Resummation in the ZZ (and W^+W^-) processes has been considered in ref. [12] at N^{2}LL+NNLO. The interface of RadISH resummation to the MATRIX program allows for N^{3}LL+NNLO resummation [7] of all diboson processes but no phenomenological results for the $W^\pm Z$ and ZZ processes at this level have been published.

In this paper we present an upgrade of CuTe-MCFM [13] which implements the SCET-based q_T resummation formalism of refs. [14–17]. We describe the N^{3}LL resummation matching to the remaining diboson processes WW, ZZ and WZ that have been recently implemented in MCFM at fixed order NNLO [18]. Our goal is to show these improvements and the phenomenological capabilities of our code, especially since the diboson calculations were previously only presented at a technical level in MCFM [18]. We present resummed results for the massive diboson processes W^+W^-, $W^\pm Z$, and WH, ZH at the level of N^{3}LL+NNLO, compare with data as far as currently available, and provide predictions for the current LHC energy of $\sqrt{s} = 13.6\,\text{TeV}$.

In addition to q_T resummation, resummation effects become important when we veto against jet activity, for example in W^+W^- production to reduce background from $t\bar{t}$ production. Although a discussion of jet-veto results is not the principal aim of our study, in view of its experimental importance we present the results of jet-veto resummation for the case of W^+W^- production. We leave a detailed analysis of jet-veto resummation of this and other processes for a future study.

In this paper we use the SCET-based "collinear anomaly" q_T resummation formalism introduced in refs. [14–16]. Formulations of q_T resummation that are fully performed in impact parameter space have the drawback that the transformation from the impact parameter space x_T back to q_T involves the running coupling at scale x_T. Therefore, when performing the Fourier transform over all values of the impact parameter, one is forced to introduce a prescription to avoid the Landau pole in the running coupling. In the formulation of refs. [14–16] this issue is avoided, setting the scale directly in q_T space.

JHEP03(2023)080

The cross-section is obtained by combining the contributions from the partonic channels $i, j \in q, \bar{q}, g$. Up to terms suppressed by powers of q_T/Q, these channels exhibit a factorized form that is fully differential in the momenta $\{q\}$ of the colorless final state

$$\begin{aligned} \mathrm{d}\sigma_{ij}(p_1, p_2, \{q\}) = & \int_0^1 \mathrm{d}z_1 \int_0^1 \mathrm{d}z_2 \, \mathrm{d}\sigma^0_{ij}(z_1 p_1, z_2 p_2, \{q\}) \, \mathcal{H}_{ij}(z_1 p_1, z_2 p_2, \{q\}, \mu) \\ & \times \frac{1}{4\pi} \int \mathrm{d}^2 x_\perp \, e^{-i q_\perp x_\perp} \left(\frac{x_T^2 Q^2}{b_0^2} \right)^{-F_{ij}(x_\perp, \mu)} \times B_i(z_1, x_\perp, \mu) \cdot B_j(z_2, x_\perp, \mu) \,, \end{aligned} \tag{1.1}$$

where p_1 and p_2 are the incoming hadron momenta. The function $\mathrm{d}\sigma^0_{ij}$ denotes the differential cross-section for the hard Born-level process and the hard-function $\mathcal{H}_{ij}$ contains the associated virtual corrections. The beam functions B_i and B_j include the effects of soft and collinear emissions at large transverse separation $x_\perp$ and the indices i and j and the momentum fractions z_1 and z_2 refer to the partons which enter the hard process after these emissions. The collinear anomaly leads to the Q^2-dependent factor within the Fourier-integral over the transverse position $x_\perp$. The perturbatively calculable anomaly exponent F_{ij} is also referred to as the rapidity anomalous dimension in the framework of ref. [32]. We further have $b_0 = 2e^{-\gamma_E}$, where γ_E is the Euler constant, and $x_T^2 = -x_\perp^2$.

This framework for q_T resummation has been implemented at N^{3}LL in CuTe-MCFM [13, 33], see ref. [13] for further details. Matching to large-q_T fixed-order predictions were previously performed at relative order α_s^2 for the processes $H, Z, W^\pm$ [34], $W^\pm H$ and ZH [35], $\gamma\gamma$ [36], $Z\gamma$ [37], as well as at N^{4}LL+N^{3}LO for Z production in ref. [38]. The code is fully differential in the Born kinematics, including the decays of the bosons and provides an efficient way to estimate uncertainties from fixed-order truncation, resummation, and parton distribution functions.

To provide phenomenologically meaningful results also for W^+W^- production, we have implemented jet-veto resummation at N^{3}LL$_\mathrm{p}$+NNLO following the collinear anomaly formalism of ref. [39]. Beam- and soft-functions are taken from refs. [40, 41] and the rapidity anomalous dimension at the two-loop level is taken from refs. [39, 42]. The notation N^{3}LL$_\mathrm{p}$ indicates that full N^{3}LL accuracy is not achieved since an approximate form, valid at small jet-radii, for the three-loop term in the collinear anomaly exponent is used [43]. A detailed presentation of our implementation and its phenomenology for various processes will be presented elsewhere [44].

2 Phenomenology

In the following we first present finely binned transverse momentum spectra at 13.6 TeV and compare fixed-order and resummation improved predictions for each diboson process. These demonstrate the impact of the N^{3}LL resummation for future analyses. In practice, in current experimental analyses the binning is still large, so that the impact of resummation is less apparent. We compare with experimental measurements as far as available for the 13 TeV LHC.

In section 2.1 we first consider ZZ production. For this process the transverse momentum of the vector boson pair system is directly measured, unlike for processes with W

JHEP03(2023)080

lepton cuts	$q_T^{l_1} > 20\,\text{GeV}$, $q_T^{l_2} > 10\,\text{GeV}$, $q_T^{l_{3,4}} > 5\,\text{GeV}$, $\lvert\eta^l\rvert < 2.5$
lepton pair mass	$60\,\text{GeV} < m_{l^-l^+} < 120\,\text{GeV}$

Table 2. Fiducial volume of the CMS ZZ analysis presented in ref. [25].

bosons which have missing energy. We compare with differential and total cross-section measurements from both CMS and ATLAS. We then present results for $W^\pm Z$ production in section 2.2 and compare with ATLAS data. Finally we present jet-veto resummed predictions for W^+W^- in section 2.3 and compare to CMS measurements. Finally, we show differential predictions at 13.6 TeV for $W^\pm H$ and ZH in section 2.4.

Input parameters. Throughout this paper we use the PDF set `NNPDF31_nnlo_as_0118` which has five active flavors, except for the W^+W^- process where we use the PDF set `NNPDF31_nnlo_as_0118_nf_4` with four active flavors [45]. We work in the electroweak G_μ scheme with $m_W = 80.385\,\text{GeV}$, $m_Z = 91.1876\,\text{GeV}$, $G_\mu = 1.166\,390 \times 10^{-5}\,\text{GeV}^{-2}$ and further have $\Gamma_W = 2.0854\,\text{GeV}$, $\Gamma_Z = 2.4952\,\text{GeV}$, $m_H = 125\,\text{GeV}$, $m_t = 173.3\,\text{GeV}$.

At fixed order we set the default renormalization and factorization scales to the invariant mass of the diboson system. For the resummation-improved results we vary hard scale, resummation scale and rapidity scale following refs. [13, 33]. We symmetrize resummation uncertainty bands to account for a frozen out downwards scale variation at small q_T that would otherwise evaluate α_s in the non-perturbative regime. Since our resummation includes the matching through a transition function, we vary this function to estimate a matching uncertainty and include this in the uncertainty bands. For the detailed procedure we refer the reader to ref. [13].

2.1 ZZ production

2.1.1 ZZ production at $\sqrt{s} = 13.6\,\text{TeV}$

We first present results for ZZ production at $\sqrt{s} = 13.6\,\text{TeV}$ using the CMS cuts in table 2 [25] to study the impact of the resummation compared to fixed order. In figure 1 we show the ZZ transverse momentum distribution at NNLO fixed-order and matched with N^{3}LL resummation. The transition region is around 30 GeV to 100 GeV and leads to uncertainties of about 15% in that region, comparable to the fixed-order uncertainties of 10%. The uncertainties in the resummation region for smaller q_T benefit from the high logarithmic accuracy until very small q_T of about 4 GeV to 5 GeV. Here resummation at the level of N^{4}LL would improve uncertainties further [38]. Overall we conclude that the central value of the resummed and fixed order results start to deviate at about 100 GeV. Within current theory uncertainty levels this difference starts to be significant at about 50 GeV.

2.1.2 Comparison with CMS measurements

We compare our predictions with the $\sqrt{s} = 13\,\text{TeV}$ CMS results of ref. [25]. The cuts for our analysis are shown in table 2. To simplify our theoretical analysis we perform

JHEP03(2023)080

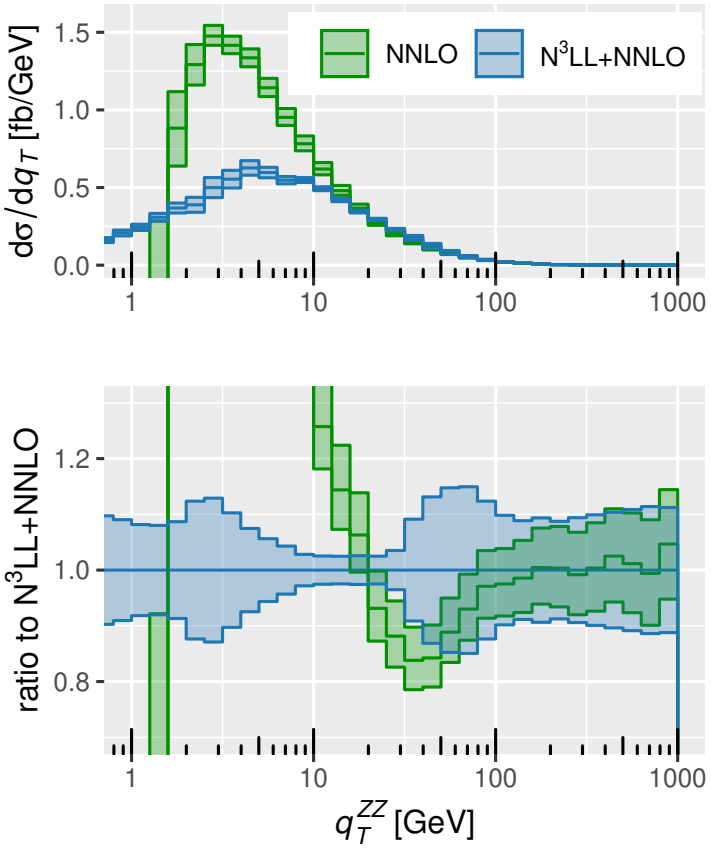

Figure 1. Transverse momentum distribution of the ZZ pair at NNLO and N^{3}LL+NNLO using the CMS cuts in table 2 [25], but at 13.6 TeV.

our calculations for Z bosons decaying to different-flavor leptons and account for all combinations with an overall factor of two. We thus neglect identical-particle effects (i.e. the $e^-e^+e^-e^+$ final state is treated in the same way as $e^-e^+\mu^-\mu^+$). We have checked that this results in a negligible difference in our results at NLO, less than two per mille, and thus the approach is fully justified.

A comparison of the fixed-order NNLO and resummed N^{3}LL+NNLO predictions for q_T^{ZZ} is shown in figure 2, also compared with the corresponding CMS data (cf. figure 5 (left) of ref. [25]). The resummation improves the description of the experimental data up to 75 GeV noticeably, as anticipated by our finely binned analysis in figure 1.

The CMS collaboration also presents a measurement of the transverse momentum of all four leptons, see figure 4 (left) of ref. [25]. Our NNLO and N^{3}LL+NNLO results for this distribution are shown in figure 3. In this distribution there is no evidence for the effects of resummation. We have therefore performed a theoretical study of the leading-lepton $q_T^{l_1}$ spectrum in figure 4, which displays the importance of resummation effects, but only at very small q_T with large uncertainties. We have checked that the distributions of the other leptons are not significantly changed by q_T resummation, which leads to this effect being washed out in the experimental measurement.

JHEP03(2023)080

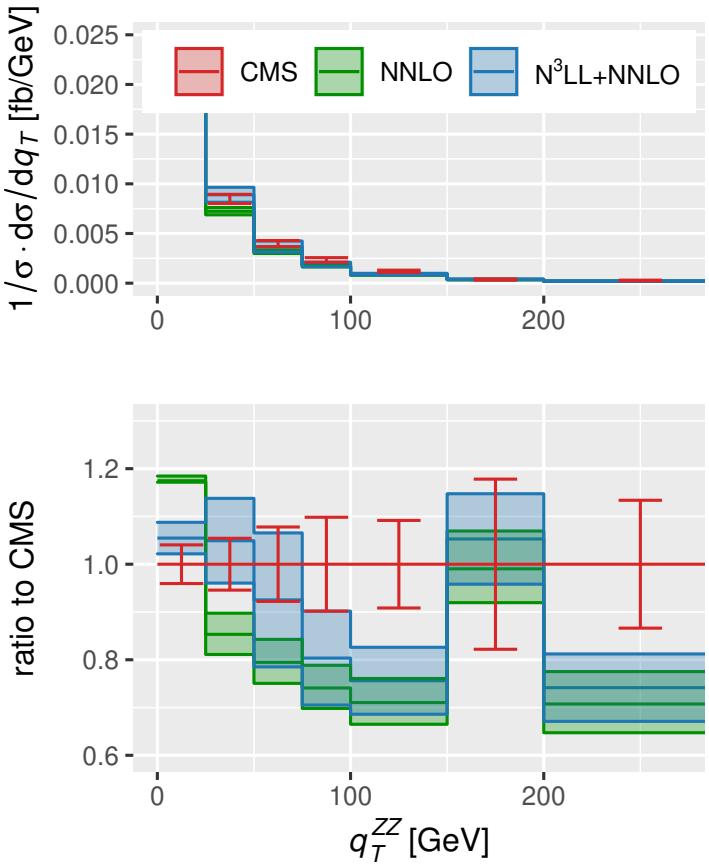

Figure 2. The q_T^{ZZ} distribution at NNLO and N^{3}LL+NNLO compared to the CMS data from ref. [25].

The resummation is based on a factorization theorem that is fully differential in the kinematics of the color-singlet system. But a lepton of a given transverse momentum can come from a vector boson pair of small transverse momentum, for which resummation yields a better prediction, or from a vector boson pair of larger transverse momentum, for which resummation will have little effect. The phenomenological impact of resummation on different lepton distributions should be studied on a case-by-case basis.

Last, we compare the total fiducial cross-section prediction with the measurement in table 3 and find reasonable agreement between theory prediction and measurement. There is little difference between the resummed and fixed-order predictions for the cross section because the lepton cuts in table 2 do not necessarily imply that the transverse momentum of the ZZ system is small.

2.1.3 Comparison with ATLAS measurements

We also compare with results from the ATLAS collaboration [24] using the cuts shown in table 4. As before, we perform our full calculations for Z bosons decaying to different-flavor leptons. Since the cuts in table 4 do not require the dilepton invariant masses to lie within a Z-mass window the effect of same-flavor interference is non-negligible. This effect can be

JHEP03(2023)080

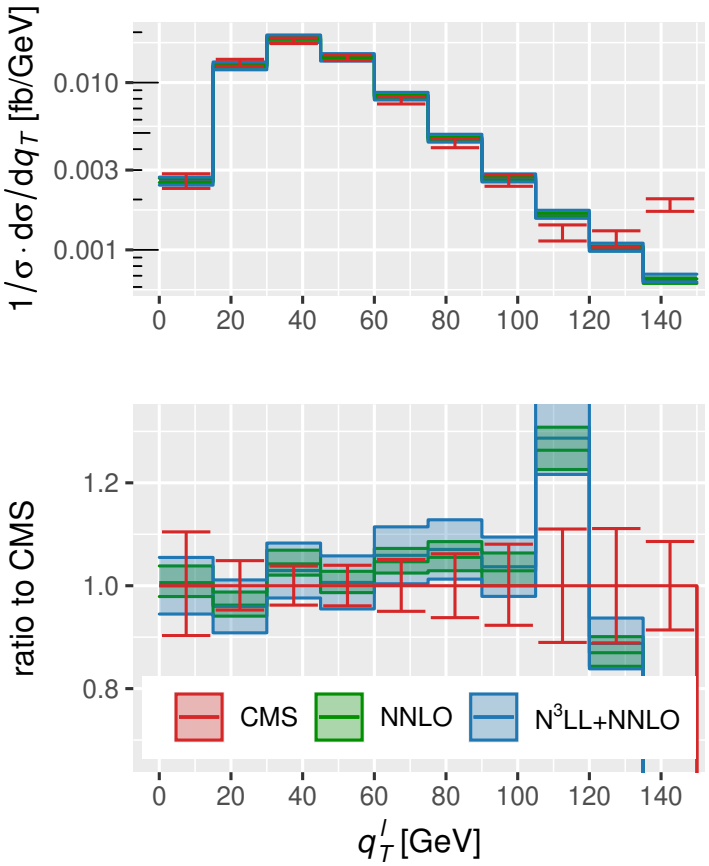

Figure 3. The q_T^l (summed over all leptons) distribution at NNLO and N^{3}LL+NNLO, compared to the CMS data from ref. [25].

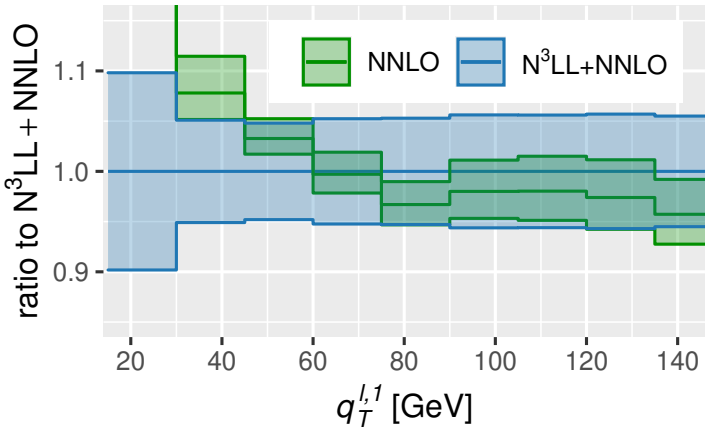

Figure 4. The $q_T^{l_1}$ distribution at NNLO as a ratio to N^{3}LL+NNLO. See figure 3 for the sum of all leptons compared to CMS data.

JHEP03(2023)080

	cross-section [fb]
NNLO	$37.8^{+0.5}_{-0.4}$ (scale)
N^{3}LL+NNLO	36.0 ± 0.8 (scale) ± 0.8 (match)
measurement	40.5 ± 0.7 (sta.) ± 1.1 (sys.) ± 0.7 (lum.)

Table 3. Comparison of total fiducial ZZ cross-section predictions at NNLO, N^{3}LL+NNLO with the CMS analysis combining measurements from 2016, 2017 and 2018 [25]. Fiducial cuts are as in table 2.

lepton cuts	$q_T^{\ell_1} > 20\,\text{GeV}$, $q_T^{\ell_2} > 10\,\text{GeV}$, $q_T^{\ell_{3,4}} > 5\,\text{GeV}$, $q_T^{e} > 7\,\text{GeV}$, $\lvert\eta^{\mu}\rvert < 2.7$, $\lvert\eta^{e}\rvert < 2.47$
lepton separation	$\Delta R(\ell, \ell') > 0.05$

Table 4. Setup for the ATLAS ZZ analysis at $\sqrt{s} = 13\,\text{TeV}$ presented in ref. [24].

measured by the ratio,

$$\frac{\sigma(4e) + \sigma(4\mu) + \sigma(2e2\mu)}{\sigma(2e2\mu)}\,. \tag{2.1}$$

In the absence of interference effects it would simply be equal to two. By explicit computation at LO and NLO we find that it is instead equal to 1.9 with this set of cuts and the procedure of ref. [24] for assigning leptons to Z-boson candidates. We therefore account for all combinations by applying this as an overall factor, thus correctly including interference contributions up to NLO but approximating them at NNLO. This is expedient in order to reduce the computational burden and, given that this ratio does not change from LO to NLO and the NNLO corrections are small, we expect only per-mille level deviations in a full calculation.

The ATLAS collaboration has performed measurements of the m_{4l} distribution in five slices of $q_T^{4\ell}$ in figure 15 of ref. [24]. We limit our comparison to the region $m_{4\ell} > 182\,\text{GeV}$ to avoid the low invariant mass region populated by $gg \to H$. Since we are resumming logarithms $\log(m_{4\ell}/q_T^{4\ell})$ our expectation is that the resummation should improve the agreement with data in the region of small $q_T^{4\ell}$, in particular as $m_{4\ell}$ increases. We show results at NNLO and N^{3}LL+NNLO in figure 5 and indeed find this expectation to be correct. For brevity we only show the comparison with the first slice $q_T^{4\ell} < 10\,\text{GeV}$.

2.2 $W^{\pm}Z$ production

2.2.1 WZ production at $\sqrt{s} = 13.6\,\text{TeV}$

We begin with predictions at 13.6 TeV for run 3 of the LHC using CMS cuts as in table 5. Figure 6 illustrates the impact that resummation has on the q_T distribution. For the purposes of illustration, q_T is constructed from the full WZ four-vector, although of course this is not a quantity that can be directly measured in experiment. Similar to the other diboson processes, the resummation becomes essential below 50 GeV to 100 GeV.

JHEP03(2023)080

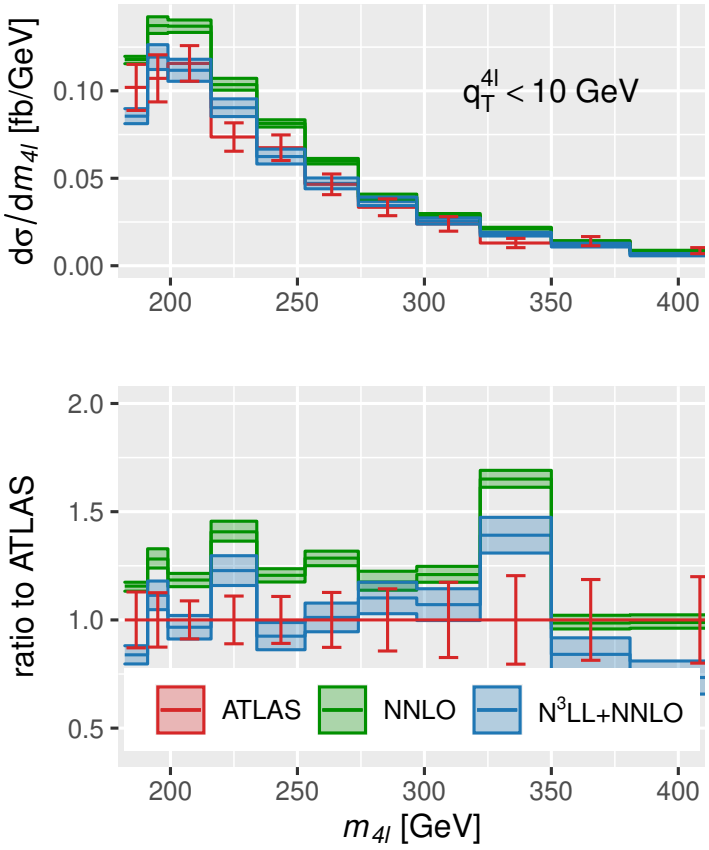

Figure 5. The m_{4l} distribution for $q_T^{4\ell} < 10\,\text{GeV}$ at NNLO and N^{3}LL+NNLO compared with ATLAS data from ref. [24].

A related quantity, which is often measured in experiment, is the transverse mass of the WZ system, m_T^{WZ}, which following ref. [19] is defined as,

$$\left(m_{\text{T}}^{WZ}\right)^2 = \left(\sum_{\ell=1}^{3} p_{\text{T}}^{\ell} + E_{\text{T}}^{\text{miss}}\right)^2 - \left[\left(\sum_{\ell=1}^{3} p_x^{\ell} + E_x^{\text{miss}}\right)^2 + \left(\sum_{\ell=1}^{3} p_y^{\ell} + E_y^{\text{miss}}\right)^2\right] . \tag{2.2}$$

The predictions for this variable are shown in figure 7. At the current level of theory uncertainties, resummation effects are relevant for transverse masses less than about 100 GeV, far below the peak region.

2.2.2 Comparison with CMS measurements

For $W^{\pm}Z$ production, we choose to focus on the CMS analysis of ref. [22]. The parameters and cuts for this study are given in table 5. We slightly simplify the theoretical analysis by computing the cross-section for different-flavor leptons only. The effect of interference in same-flavor final states is measured by the ratio,

$$\frac{\sigma(3e) + \sigma(3\mu) + \sigma(2e,\mu) + \sigma(2\mu,e)}{\sigma(2e,\mu)} . \tag{2.3}$$

JHEP03(2023)080

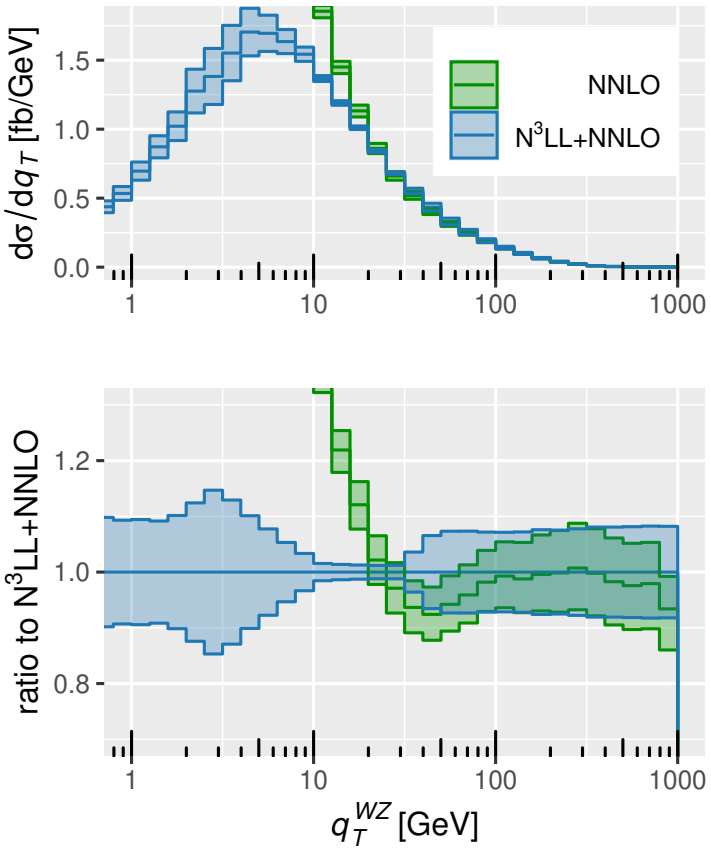

Figure 6. Comparison of NNLO and N^{3}LL+NNLO predictions for truth $p_T^{W^\pm Z}$ at 13.6 TeV using the CMS cuts in table 5.

lepton cuts	$p_T^{\ell_{Z1}} > 25\,\text{GeV}$, $p_T^{\ell_{Z2}} > 10\,\text{GeV}$, $p_T^{\ell_W} > 25\,\text{GeV}$, $\lvert\eta^\ell\rvert < 2.5$, $60\,\text{GeV} < m_{\ell^-\ell^+} < 120\,\text{GeV}$, $M(\ell_{Z1}, \ell_{Z2}, \ell_W) > 100\,\text{GeV}$

Table 5. Setup for the CMS WZ fiducial volume analysis at $\sqrt{s} = 13\,\text{TeV}$ presented in ref. [22].

Without identical-particle interference this would be equal to four, but we instead find a value of 4.06 at LO and NLO under this set of cuts and the procedure of ref. [22] for assigning leptons to W and Z-boson candidates. We therefore sum over lepton flavors by applying this overall factor to the NNLO calculation of the different-flavor final state.

We first compare total fiducial cross-sections in table 6 and find excellent agreement between theory prediction and measurement within uncertainties. Similar to the case of ZZ production, the resummed and fixed-order predictions agree within uncertainties due to the fact that the cuts of table 5 are relatively inclusive and do not preferentially select the region of small q_T^{WZ}.

JHEP03(2023)080

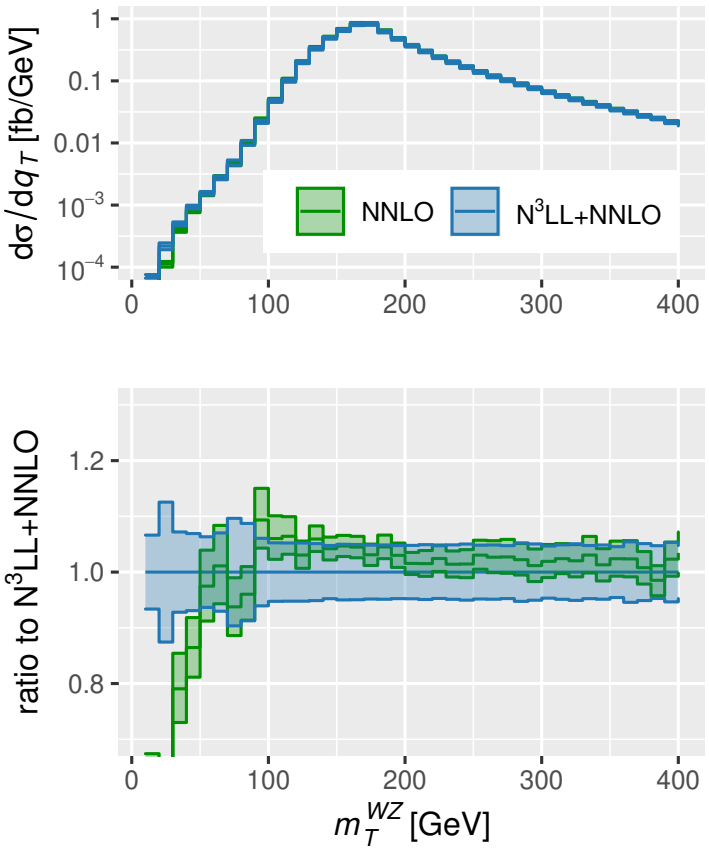

Figure 7. Comparison of NNLO and N^{3}LL+NNLO predictions for the truth $m_T^{W^\pm Z}$ at 13.6 TeV using the CMS cuts in table 5.

	$W^-Z \to e^-\bar{\nu}\mu^-\mu^+$ [fb]	$W^+Z \to e^+\nu\mu^-\mu^+$ [fb]
NNLO	$30.3^{+0.7}_{-0.6}$	$43.4^{+0.9}_{-0.9}$
N^{3}LL+NNLO	$29.4 \pm 1.1\,(\text{scale}) \pm 0.3\,(\text{match.})$	$42.2 \pm 1.5\,(\text{scale}) \pm 0.4\,(\text{match.})$
measurement	$31.8 \pm 1.4\,(\text{sta.}) \pm 1.1\,(\text{sys.}) \pm 0.6\,(\text{lum.})$	$43.1 \pm 1.4\,(\text{sta.}) \pm 1.5\,(\text{sys.}) \pm 0.9\,(\text{lum.})$

Table 6. Comparison of total fiducial WZ cross-section predictions at NNLO, N^{3}LL+NNLO with the CMS measurements taken from tables 8 and 9 of ref. [22]. Fiducial cuts are as in table 5.

We then turn to the differential comparison with the measurement of ref. [22]. The transverse momentum distribution of the lepton from the decay of the W (summed over both charges) is shown at NNLO and N^{3}LL+NNLO in figure 8. It is important to note that small recoils of the $W^\pm Z$ system do not always result in small recoils of the individual leptons. Therefore, the impact of transverse momentum resummation can differ phenomenologically. Based on the results from the ZZ system, we know that the leading lepton's q_T is strongly correlated with the ZZ q_T, thus receiving the largest corrections from resummation. However, in the case of the W decay, the lepton does not have to be the leading one, thus the effects are diluted.

JHEP03(2023)080

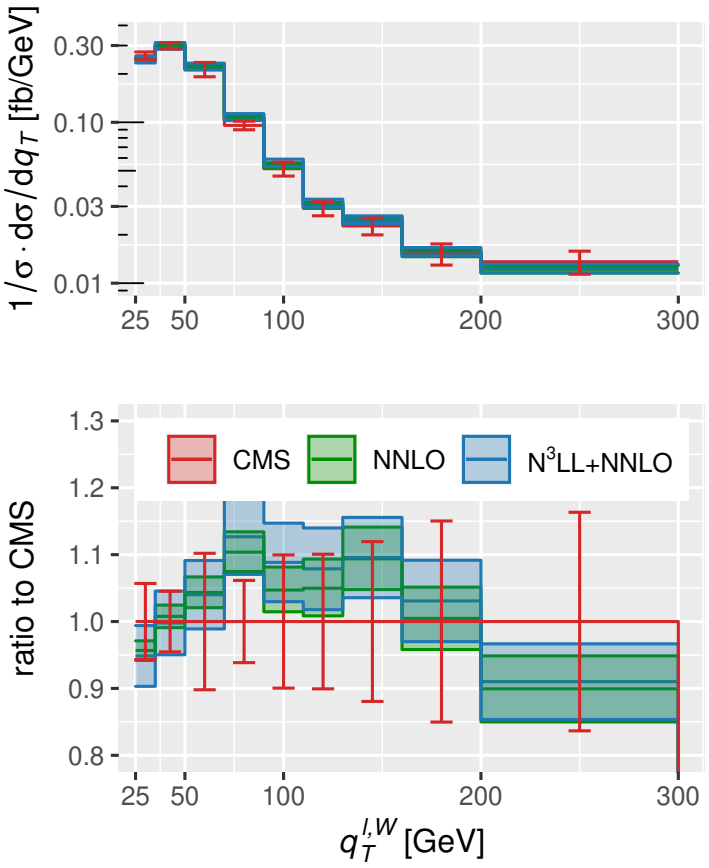

Figure 8. The $q_T^{\ell_W}$ distribution for $W^{\pm}Z$ at NNLO and N^{3}LL+NNLO compared to the CMS data from ref. [22].

2.3 W^+W^- production

The experimental study of W^+W^- production is subject to large backgrounds, principally from top production, but also from Drell-Yan processes, W+jet production, and other di- and tri-boson production processes. Reducing the background from top production to an acceptable level currently requires the imposition of a veto on jet activity. We have implemented jet-veto resummation for all single boson and boson pair processes at the level of N^{3}LL$_{\rm p}$+NNLO based on the collinear anomaly formalism [39] and the ingredients available in the literature [40, 41]. Here we only present results for W^+W^- production and leave a detailed jet-veto study for a future publication [44]. Previous detailed analyses of this process in the literature are at the level of N^{2}LL [7, 8, 10] and N^{3}LL$_{\rm p}$+NNLO [9]. Our implementation of the jet veto resummation is closer to full N^{3}LL+NNLO than ref. [9], since it contains complete results for the beam function [41], including dependence on the jet radius R.

We will compare our jet-veto resummed predictions to results from a CMS analysis at $\sqrt{s} = 13\,\text{TeV}$ [28] that are obtained using the cuts in table 7. Our calculation is performed using the $n_f = 4$ version of the PDFs to ensure consistency across the entire calculation. In order to sum over both electrons and muons we have to take care that the

JHEP03(2023)080

lepton cuts	$q_T^\ell > 20\,\text{GeV}$, $\lvert\eta^\ell\rvert < 2.5$,
	$m_{\ell\ell} > 20\,\text{GeV}$, $q_T^{\ell\ell} > 30\,\text{GeV}$,
	$q_T^{\text{miss}} > 30\,\text{GeV}$
jet veto	anti-k_T, $R = 0.4$, 0-jet events only

Table 7. Setup for the CMS W^+W^- fiducial volume analysis at $\sqrt{s} = 13\,\text{TeV}$ presented in ref. [28].

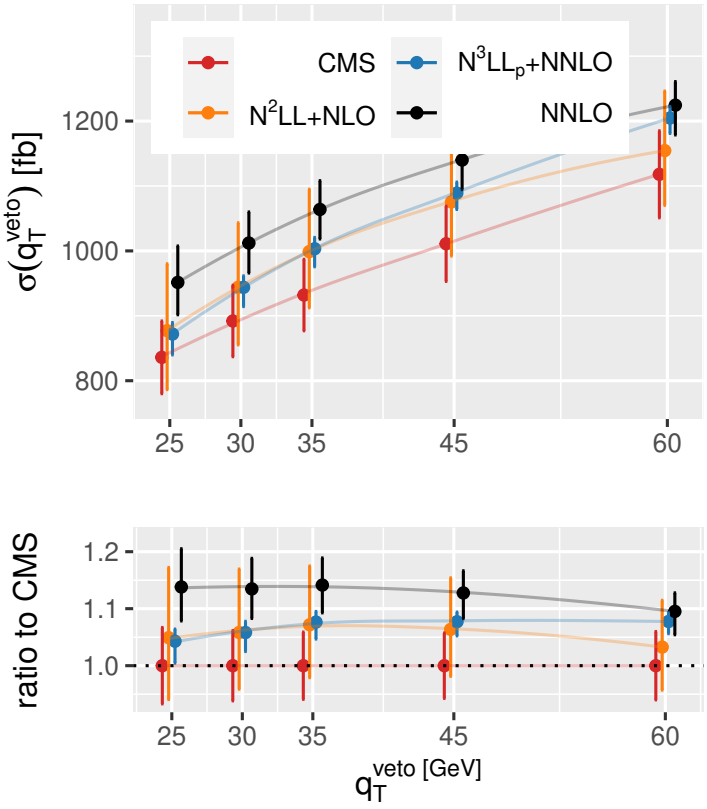

Figure 9. Jet-veto resummed cross-sections for $W^+W^- \to 2e2\nu$ production at 13 TeV using the CMS cuts in table 7 of this section in comparison with the CMS measurement [28]. The solid lines are interpolations to guide the eye.

final state $e^-\bar{\nu}_e e^+\bar{\nu}_e$ is properly included in the calculation. Although contributions of the form $ZZ \to e^-\bar{\nu}_e e^+\bar{\nu}_e$ are negligible if a suitable cut on $|m_{\ell\bar{\ell}} - m_Z|$ is applied, the CMS results reported in table 6 of ref. [28] do not include such a cut.[1] At NLO we find,

$$\frac{\sigma(e^-\bar{\nu}_e e^+\bar{\nu}_e) + \sigma(\mu^-\bar{\nu}_\mu \mu^+\bar{\nu}_\mu) + \sigma(\mu^-\bar{\nu}_\mu e^+\bar{\nu}_e) + \sigma(e^-\bar{\nu}_e \mu^+\bar{\nu}_\mu)}{\sigma(\mu^-\bar{\nu}_\mu e^+\bar{\nu}_e)} = 4.15\,, \tag{2.4}$$

independent of the value of q_T^{veto} in the range studied here. Without the additional same-flavor contribution from ZZ diagrams this would just be equal to four. To simplify our NNLO prediction, we compute the different-flavor cross-section at this order and multiply

[1] We thank Pietro Govoni for clarification of this point.

JHEP03(2023)080

by a factor of 4.15 instead. We include the gg channel at leading fixed order. For simplicity we do not include a transition function for this calculation but perform a naive matching.

Our predictions, and a comparison with the CMS results of ref. [28], are shown in figure 9. The matched resummed cross-sections are dominated by the resummed part, with 5 to 10 percent matching corrections between $q_T^{\text{veto}} = 25\,\text{GeV}$ and $60\,\text{GeV}$. There is general agreement between these predictions and measurements but fixed-order NNLO predictions differ by a larger amount, highlighting the need for jet-veto resummed results. To obtain robust predictions for the jet-vetoed NNLO results we use the value of the jet-veto for the central resummation and factorization scales and include a factor two variation about them to estimate uncertainties.

2.4 WH and ZH production

Matched N^{3}LL+NNLO calculations for WH and ZH were implemented in ref. [13], but no results were presented. Here we present predictions for these two processes at $\sqrt{s} = 13.6\,\text{TeV}$ to demonstrate the capabilities of the code. For this demonstration we do not apply cuts on the electroweak final state after W, Z and H bosons decay. We further divide out the branching ratio to give the total rate independent of the particular decay channel.

We have also upgraded our code to include resummation for $W\gamma$ production, but do not show results, since $Z\gamma$ has been extensively discussed in ref. [13]. In particular, the issue of photon isolation plays a big role in this process and requires a dedicated discussion.

3 Conclusions

The experimental study of massive diboson kinematics is still in its infancy. Currently only 5% of the final LHC luminosity has been recorded and the high-luminosity LHC will require precise predictions at the percent level. We have presented transverse momentum resummed results at the level of N^{3}LL+NNLO for the production of pairs of vector bosons ZZ, $W^{\pm}Z$, $W^{\pm}H$ and ZH. Where experimental data has been available in sufficient detail we have shown that the inclusion of the resummed logarithms leads to improved agreement with the data at low q_T. For W^+W^- production we have shown jet-veto resummed predictions in comparison with measurements and find agreement within uncertainties.

Current binning of experimental data is not fine-grained and still quite inclusive. In particular one often has a large first bin starting at $q_T = 0$. This diminishes the effect of q_T resummation, which is most necessary at the differential level at small q_T, but also for certain sets of fiducial cuts at an inclusive level at a sufficient level of precision [46]. Our more finely binned predictions for $\sqrt{s} = 13.6\,\text{TeV}$ show the importance of resummation when precise enough data becomes available.

With decreasing experimental uncertainties it will be necessary to take into account NLO corrections to the gg channel [47, 48], which we only include at LO, as well as NLO electroweak corrections [49–51] that can be included by the use of automated one-loop tools [49, 52, 53].

Our calculation will be publicly available in the upcoming release of MCFM and can be used to reproduce the results in this study as well as to perform further studies with

JHEP03(2023)080

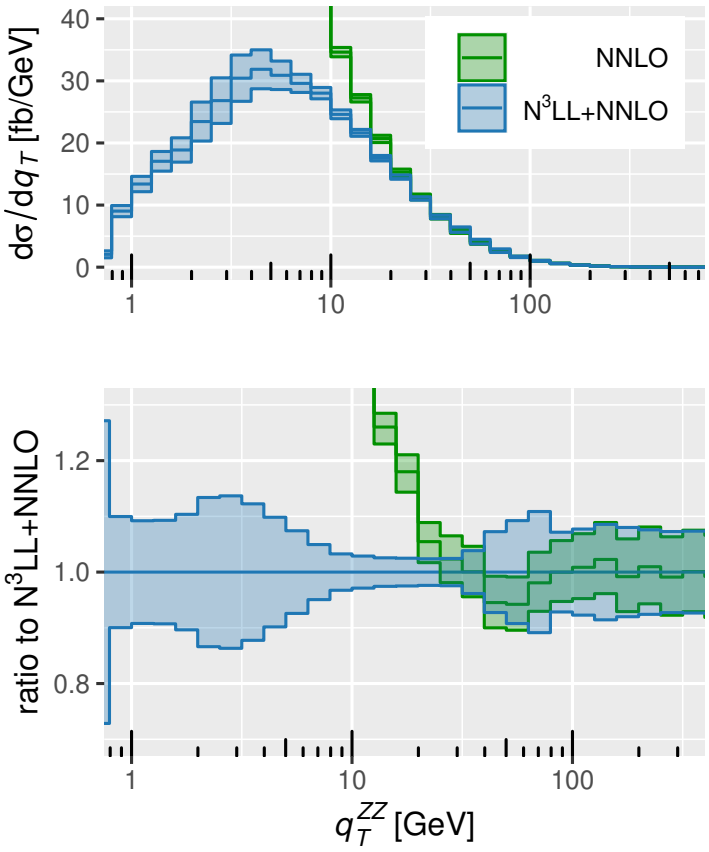

Figure 10. The q_T^{WH} distribution for $W^+H + W^-H$ at N^{3}LL+NNLO compared to fixed order NNLO.

modified parameters. With this, our calculation also provides an important theoretical tool for comparison and tuning of approaches based on parton shower event generators operating at low logarithmic accuracy.

Acknowledgments

This manuscript has been authored by Fermi Research Alliance, LLC under Contract No. DE-AC02-07CH11359 with the U.S. Department of Energy, Office of Science, Office of High Energy Physics (JMC). TN is supported by the United States Department of Energy under Grant Contract DE-SC0012704. This research used resources of the National Energy Research Scientific Computing Center (NERSC), a U.S. Department of Energy Office of Science User Facility located at Lawrence Berkeley National Laboratory, operated under Contract No. DE-AC02-05CH11231 using NERSC award HEP-ERCAP0021890.

JHEP03(2023)080

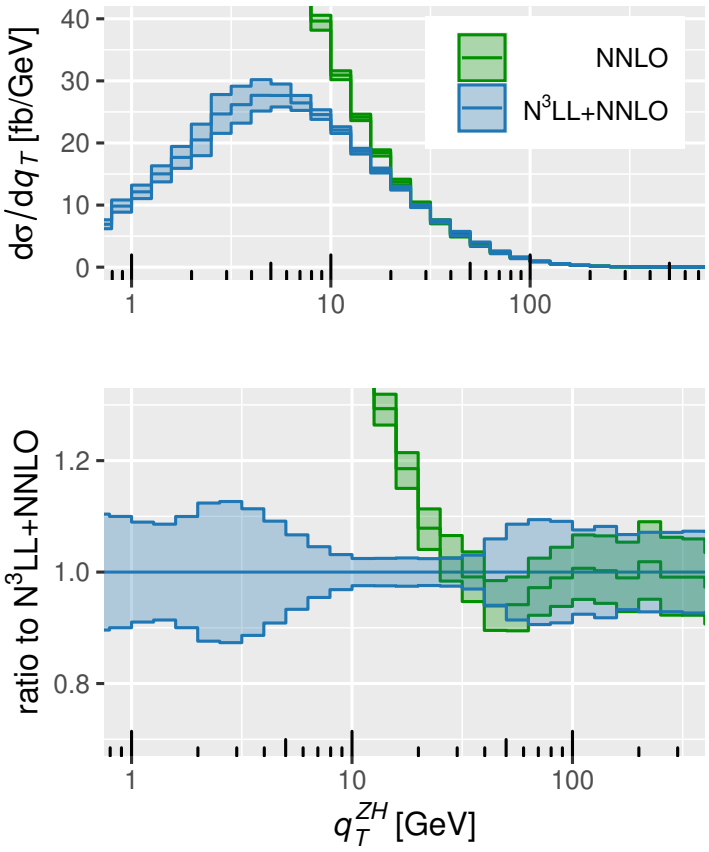

Figure 11. The q_T^{ZH} distribution at N^{3}LL+NNLO compared to fixed order NNLO.

References

[1] CMS collaboration, *Observation of the production of three massive gauge bosons at* $\sqrt{s} = 13$ *TeV*, *Phys. Rev. Lett.* **125** (2020) 151802 [arXiv:2006.11191] [INSPIRE].

[2] CMS collaboration, *Search for the production of* $W^{\pm}W^{\pm}W^{\mp}$ *events at* $\sqrt{s} = 13$ *TeV*, *Phys. Rev. D* **100** (2019) 012004 [arXiv:1905.04246] [INSPIRE].

[3] ATLAS collaboration, *Evidence for the production of three massive vector bosons with the ATLAS detector*, *Phys. Lett. B* **798** (2019) 134913 [arXiv:1903.10415] [INSPIRE].

[4] M. Grazzini, *Soft-gluon effects in WW production at hadron colliders*, *JHEP* **01** (2006) 095 [hep-ph/0510337] [INSPIRE].

[5] P. Meade, H. Ramani and M. Zeng, *Transverse momentum resummation effects in* W^+W^- *measurements*, *Phys. Rev. D* **90** (2014) 114006 [arXiv:1407.4481] [INSPIRE].

[6] W. Bizon et al., *Momentum-space resummation for transverse observables and the Higgs* $p_\perp$ *at* $N^3LL+NNLO$, *JHEP* **02** (2018) 108 [arXiv:1705.09127] [INSPIRE].

[7] S. Kallweit, E. Re, L. Rottoli and M. Wiesemann, *Accurate single- and double-differential resummation of colour-singlet processes with MATRIX+RADISH:* W^+W^- *production at the LHC*, *JHEP* **12** (2020) 147 [arXiv:2004.07720] [INSPIRE].

JHEP03(2023)080

[8] P. Jaiswal and T. Okui, *Explanation of the WW excess at the LHC by jet-veto resummation*, *Phys. Rev. D* **90** (2014) 073009 [arXiv:1407.4537] [INSPIRE].

[9] S. Dawson et al., *Resummation of jet veto logarithms at N^3LL_a+NNLO for W^+W^- production at the LHC*, *Phys. Rev. D* **94** (2016) 114014 [arXiv:1606.01034] [INSPIRE].

[10] L. Arpino, A. Banfi, S. Jäger and N. Kauer, *BSM WW production with a jet veto*, *JHEP* **08** (2019) 076 [arXiv:1905.06646] [INSPIRE].

[11] Y. Wang et al., *Transverse-momentum resummation for gauge boson pair production at the hadron collider*, *Phys. Rev. D* **88** (2013) 114017 [arXiv:1307.7520] [INSPIRE].

[12] M. Grazzini, S. Kallweit, D. Rathlev and M. Wiesemann, *Transverse-momentum resummation for vector-boson pair production at NNLL+NNLO*, *JHEP* **08** (2015) 154 [arXiv:1507.02565] [INSPIRE].

[13] T. Becher and T. Neumann, *Fiducial q_T resummation of color-singlet processes at N^3LL+NNLO*, *JHEP* **03** (2021) 199 [arXiv:2009.11437] [INSPIRE].

[14] T. Becher and M. Neubert, *Drell-Yan production at small q_T, transverse parton distributions and the collinear anomaly*, *Eur. Phys. J. C* **71** (2011) 1665 [arXiv:1007.4005] [INSPIRE].

[15] T. Becher, M. Neubert and D. Wilhelm, *Electroweak gauge-boson production at small q_T: infrared safety from the collinear anomaly*, *JHEP* **02** (2012) 124 [arXiv:1109.6027] [INSPIRE].

[16] T. Becher, M. Neubert and D. Wilhelm, *Higgs-boson production at small transverse momentum*, *JHEP* **05** (2013) 110 [arXiv:1212.2621] [INSPIRE].

[17] T. Becher and M. Hager, *Event-based transverse momentum resummation*, *Eur. Phys. J. C* **79** (2019) 665 [arXiv:1904.08325] [INSPIRE].

[18] J.M. Campbell, R.K. Ellis and S. Seth, *Non-local slicing approaches for NNLO QCD in MCFM*, *JHEP* **06** (2022) 002 [arXiv:2202.07738] [INSPIRE].

[19] ATLAS collaboration, *Measurement of $W^\pm Z$ production cross sections and gauge boson polarisation in pp collisions at $\sqrt{s} = 13$ TeV with the ATLAS detector*, *Eur. Phys. J. C* **79** (2019) 535 [arXiv:1902.05759] [INSPIRE].

[20] CMS collaboration, *Measurements of the $pp \to WZ$ inclusive and differential production cross section and constraints on charged anomalous triple gauge couplings at $\sqrt{s} = 13$ TeV*, *JHEP* **04** (2019) 122 [arXiv:1901.03428] [INSPIRE].

[21] CMS collaboration, *Search for anomalous triple gauge couplings in WW and WZ production in lepton + jet events in proton-proton collisions at $\sqrt{s} = 13$ TeV*, *JHEP* **12** (2019) 062 [arXiv:1907.08354] [INSPIRE].

[22] CMS collaboration, *Measurement of the inclusive and differential WZ production cross sections, polarization angles, and triple gauge couplings in pp collisions at $\sqrt{s} = 13$ TeV*, *JHEP* **07** (2022) 032 [arXiv:2110.11231] [INSPIRE].

[23] ATLAS collaboration, *Measurement of ZZ production in the $\ell\ell\nu\nu$ final state with the ATLAS detector in pp collisions at $\sqrt{s} = 13$ TeV*, *JHEP* **10** (2019) 127 [arXiv:1905.07163] [INSPIRE].

[24] ATLAS collaboration, *Measurements of differential cross-sections in four-lepton events in 13 TeV proton-proton collisions with the ATLAS detector*, *JHEP* **07** (2021) 005 [arXiv:2103.01918] [INSPIRE].

JHEP03(2023)080

[25] CMS collaboration, *Measurements of $pp \to ZZ$ production cross sections and constraints on anomalous triple gauge couplings at $\sqrt{s} = 13$ TeV*, *Eur. Phys. J. C* **81** (2021) 200 [arXiv:2009.01186] [INSPIRE].

[26] ATLAS collaboration, *Measurement of the W^+W^- production cross section in pp collisions at a centre-of-mass energy of $\sqrt{s} = 13$ TeV with the ATLAS experiment*, *Phys. Lett. B* **773** (2017) 354 [arXiv:1702.04519] [INSPIRE].

[27] ATLAS collaboration, *Measurement of fiducial and differential W^+W^- production cross-sections at $\sqrt{s} = 13$ TeV with the ATLAS detector*, *Eur. Phys. J. C* **79** (2019) 884 [arXiv:1905.04242] [INSPIRE].

[28] CMS collaboration, *W^+W^- boson pair production in proton-proton collisions at $\sqrt{s} = 13$ TeV*, *Phys. Rev. D* **102** (2020) 092001 [arXiv:2009.00119] [INSPIRE].

[29] ATLAS collaboration, *Measurements of WH and ZH production in the $H \to b\bar{b}$ decay channel in pp collisions at 13 TeV with the ATLAS detector*, *Eur. Phys. J. C* **81** (2021) 178 [arXiv:2007.02873] [INSPIRE].

[30] ATLAS collaboration, *Measurement of the associated production of a Higgs boson decaying into b-quarks with a vector boson at high transverse momentum in pp collisions at $\sqrt{s} = 13$ TeV with the ATLAS detector*, *Phys. Lett. B* **816** (2021) 136204 [arXiv:2008.02508] [INSPIRE].

[31] CMS collaboration, *Observation of Higgs boson decay to bottom quarks*, *Phys. Rev. Lett.* **121** (2018) 121801 [arXiv:1808.08242] [INSPIRE].

[32] J.-Y. Chiu, A. Jain, D. Neill and I.Z. Rothstein, *A formalism for the systematic treatment of rapidity logarithms in quantum field theory*, *JHEP* **05** (2012) 084 [arXiv:1202.0814] [INSPIRE].

[33] T. Neumann, *The diphoton q_T spectrum at N^3LL'+NNLO*, *Eur. Phys. J. C* **81** (2021) 905 [arXiv:2107.12478] [INSPIRE].

[34] R. Boughezal et al., *Color singlet production at NNLO in MCFM*, *Eur. Phys. J. C* **77** (2017) 7 [arXiv:1605.08011] [INSPIRE].

[35] J.M. Campbell, R.K. Ellis and C. Williams, *Associated production of a Higgs boson at NNLO*, *JHEP* **06** (2016) 179 [arXiv:1601.00658] [INSPIRE].

[36] J.M. Campbell, R.K. Ellis, Y. Li and C. Williams, *Predictions for diphoton production at the LHC through NNLO in QCD*, *JHEP* **07** (2016) 148 [arXiv:1603.02663] [INSPIRE].

[37] J.M. Campbell, T. Neumann and C. Williams, *$Z\gamma$ production at NNLO including anomalous couplings*, *JHEP* **11** (2017) 150 [arXiv:1708.02925] [INSPIRE].

[38] T. Neumann and J. Campbell, *Fiducial Drell-Yan production at the LHC improved by transverse-momentum resummation at N^4LL_p+N^3LO*, *Phys. Rev. D* **107** (2023) L011506 [arXiv:2207.07056] [INSPIRE].

[39] T. Becher, M. Neubert and L. Rothen, *Factorization and N^3LL_p+NNLO predictions for the Higgs cross section with a jet veto*, *JHEP* **10** (2013) 125 [arXiv:1307.0025] [INSPIRE].

[40] S. Abreu, J.R. Gaunt, P.F. Monni and R. Szafron, *The analytic two-loop soft function for leading-jet p_T*, *JHEP* **08** (2022) 268 [arXiv:2204.02987] [INSPIRE].

[41] S. Abreu et al., *Quark and gluon two-loop beam functions for leading-jet p_T and slicing at NNLO*, arXiv:2207.07037 [CERN-TH-2022-118] [INSPIRE].

JHEP03(2023)080

[42] A. Banfi, P.F. Monni, G.P. Salam and G. Zanderighi, *Higgs and Z-boson production with a jet veto*, *Phys. Rev. Lett.* **109** (2012) 202001 [arXiv:1206.4998] [INSPIRE].

[43] A. Banfi et al., *Jet-vetoed Higgs cross section in gluon fusion at N^3LO+NNLL with small-R resummation*, *JHEP* **04** (2016) 049 [arXiv:1511.02886] [INSPIRE].

[44] J.M. Campbell, R.K. Ellis, T. Neumann and S. Seth, *Jet-veto resummation at N^3LL_p+NNLO in boson production processes*, arXiv:2301.11768 [INSPIRE].

[45] NNPDF collaboration, *Parton distributions from high-precision collider data*, *Eur. Phys. J. C* **77** (2017) 663 [arXiv:1706.00428] [INSPIRE].

[46] G.P. Salam and E. Slade, *Cuts for two-body decays at colliders*, *JHEP* **11** (2021) 220 [arXiv:2106.08329] [INSPIRE].

[47] M. Grazzini, S. Kallweit, M. Wiesemann and J.Y. Yook, *W^+W^- production at the LHC: NLO QCD corrections to the loop-induced gluon fusion channel*, *Phys. Lett. B* **804** (2020) 135399 [arXiv:2002.01877] [INSPIRE].

[48] M. Grazzini, S. Kallweit, M. Wiesemann and J.Y. Yook, *ZZ production at the LHC: NLO QCD corrections to the loop-induced gluon fusion channel*, *JHEP* **03** (2019) 070 [arXiv:1811.09593] [INSPIRE].

[49] S. Kallweit et al., *NLO electroweak automation and precise predictions for W+multijet production at the LHC*, *JHEP* **04** (2015) 012 [arXiv:1412.5157] [INSPIRE].

[50] S. Kallweit, J.M. Lindert, S. Pozzorini and M. Schönherr, *NLO QCD+EW predictions for $2\ell 2\nu$ diboson signatures at the LHC*, *JHEP* **11** (2017) 120 [arXiv:1705.00598] [INSPIRE].

[51] M. Grazzini et al., *NNLO QCD+NLO EW with Matrix+OpenLoops: precise predictions for vector-boson pair production*, *JHEP* **02** (2020) 087 [arXiv:1912.00068] [INSPIRE].

[52] S. Actis et al., *RECOLA: REcursive Computation of One-Loop Amplitudes*, *Comput. Phys. Commun.* **214** (2017) 140 [arXiv:1605.01090] [INSPIRE].

[53] M. Chiesa, N. Greiner and F. Tramontano, *Automation of electroweak corrections for LHC processes*, *J. Phys. G* **43** (2016) 013002 [arXiv:1507.08579] [INSPIRE].

JHEP03(2023)080